# Chapter 2

# Materials and Methods

## 2.1. Introduction

This chapter discusses the techniques of different materials synthesis processes, materials characterizations, and electrochemical/photocatalysis measurement processes, which were adopted for this series of work presented in this thesis. All of these discussions are based on the review of past results presented in chapter 1 and the experimental equipment accessible in our laboratory. These studies are meant to create and refine the electrocatalysts to deliver a high-performing two-dimensional nanomaterial-based catalyst with suitable structural architecture.

The following sections will provide more explanation in greater depth, such as hydrothermal synthesis of the 2D-$MoS_2$ nanosheets, $MoNi_4/MoO_2$ nanorods, $MoNi_4/MoO_2$:rGO nanocomposite, $MoS_2$:$MoNi_4/MoO_2$ nanohybrid, $SO_3H$ functionalized $MoS_2$ nanosheets, $SO_3H/SO_3$ functionalized $MoS_2$, and graphene oxide (GO) synthesis by using the modified hummer's method, etc. All the experimental techniques are discussed here, along with the various processing/synthesis parameters. All the materials characterization techniques are discussed with the instrumental set-ups, arrangements of experimentations, and parameters. The characterizations include x-ray powder diffraction (XRD), field-emission (FE)/high-resolution(HR) scanning electron microscopy (SEM), transmission electron microscopy/ high-resolution transmission electron microscopy (TEM/HRTEM), X-ray photoemission spectroscopy (XPS), Raman spectroscopy, Fourier transform infrared spectroscopy (FTIR), Ultraviolet-visible spectroscopy (UV-Vis), thermogravimetric analysis (TGA), differential scanning calorimetry (DSC) and Brunauer-Emmett-Teller (BET), contact-angle measurements, etc. For demonstrating applications of as-develop materials, photocatalysis measurements and a series of electrochemical measurements were performed and discussed in this chapter as follows.

### 2.1.1 Hydrothermal synthesis (HTS)

Hydrothermal synthesis (HTS) is an essential part of inorganic synthesis in an aqueous medium using a sealed vessel at high pressure (1-100 MPa) and temperature (100 to 1000 ºC). All the HTS reactions for these works were performed in a hydrothermal autoclave composed of (1) high-quality thick-walled stainless steel and (2) a 100 mL Teflon autoclave. The Teflon-lined autoclave allows reaction at a maximum temperature of 250 ºC, while the reproducibility of HTS reactions strictly depends on the volume fraction of solution used in the container. In general, the Teflon vessels are filled between 60 to 80% for the standard chemical reaction to set up pressure between 0.02-0.3 GPa. Figure 2.1a shows a typical Teflon-lined autoclave, which was used for almost all the reactions discussed in this work. Figure 2.1b and Figure 2.1c demonstrate the laboratory oven and the atmospheric-controlled tube furnace, respectively, which were used for performing various experiments for this research work.

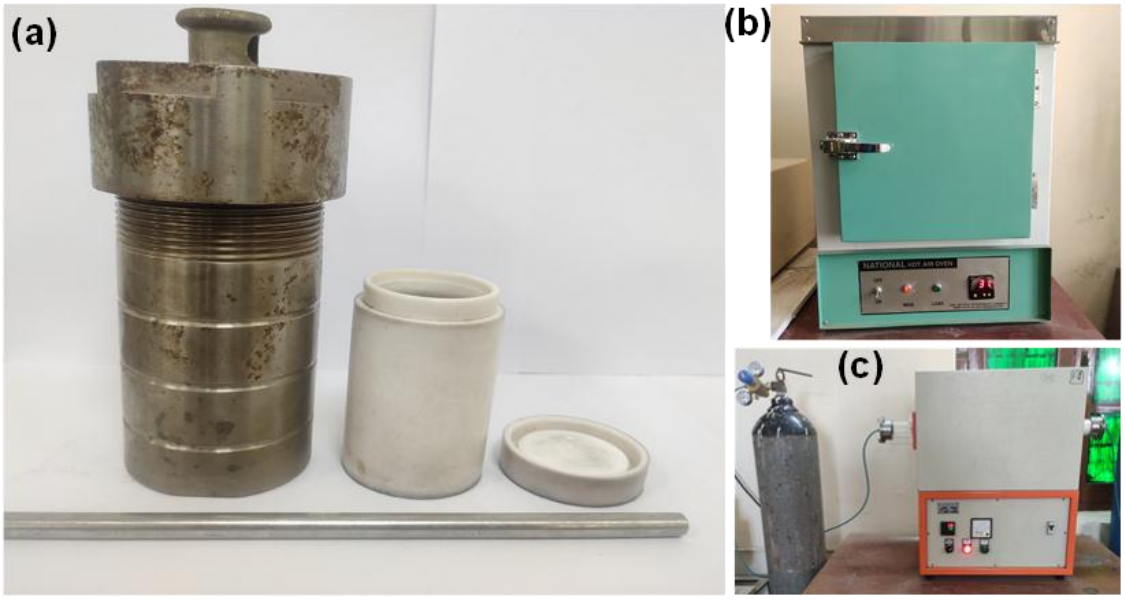


***Figure 2.1:*** *Shows (a) Autoclave used for hydrothermal synthesis; (b) laboratory vacuum oven, and (c) atmospheric controlled laboratory tube furnace, which were used for all the synthesis processes for this work.*

### 2.1.2 Synthesis of $MoNi_4/MoO_2$ nanorods

The $MoNi_4/MoO_2$ nanorods were synthesized in various steps, where 0.01 M ammonium molybdate tetrahydrate ($(NH_4)_6Mo_7O_{24}\cdot 4H_2O$) and 0.04 M Nickel (II) nitrate hexahydrate ($Ni(NO_3)_2\cdot 6H_2O$) were dissolved in 30 mL of DI water as shown in Figure 2.2 [1]. Then, the solution was stirred for 20 min at 400 rpm to get a homogeneous mixture. After that, the mixed solution was transferred to a 50 mL Teflon-lined autoclave and heat-treated at 150 °C for 6 h inside of a laboratory hot-air oven. Once the reaction was over, the autoclave was allowed to naturally cool down at room temperature, and after cooling, the solution was washed two to three times using DI water and ethanol, followed by drying at 80 °C for 12 h inside a vacuum oven to obtain the $MoNi_4/MoO_2$ nanorod powder. The as-synthesized powder was heat-treated in an environmentally controlled laboratory quartz tube furnace at 500 °C for 2 h in the presence of an $H_2$:$N_2$ (5:95) gas mixture environment to obtain nano dispersed $MoNi_4$ embedded in $MoO_2$ nanorods.

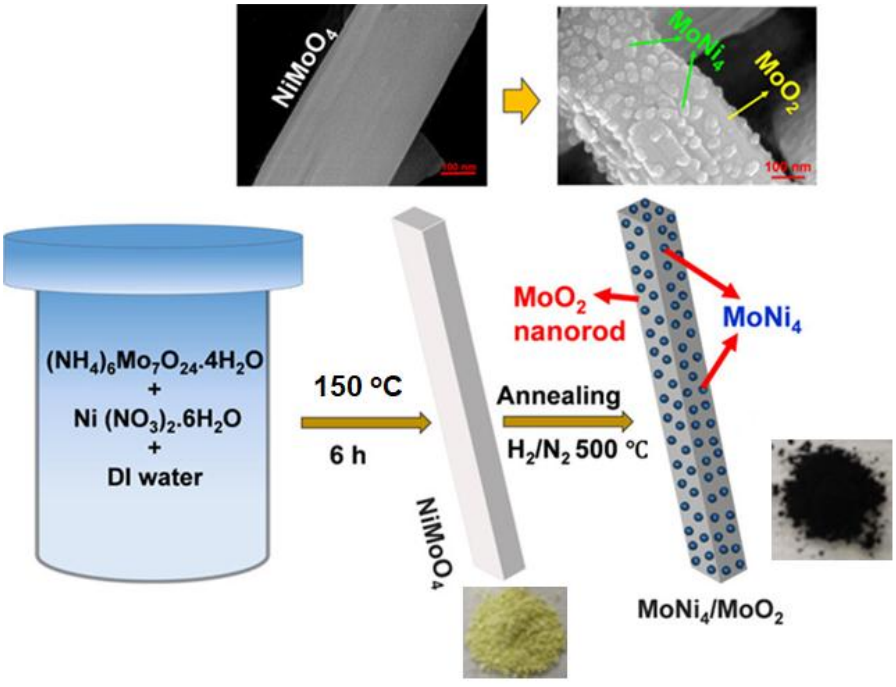


***Figure 2.2:*** Schematic of the $MoNi_4/MoO_2$ nanorod synthesized by a one-pot hydrothermal process.

### 2.1.3 Graphene oxide (GO) synthesis via modified Hummers' method

Figure 2.3 shows the step-by-step synthesis of graphene oxide (GO), and reduced graphene oxide (rGO) by using the modified Hummers' method [2, 3]. In this process, 1:9 mixture of concentrated $H_3PO_4/H_2SO_4$ (40:360 ml) solution was added to a mixture of $KMnO_4$ (18g) and graphite flakes (3g), and the reaction was then heated to 80 ºC and stirred for 12 h until the solution became dark green. The reaction was cooled down to room temperature (RT) and poured onto ice cubes of deionized water (DI water) slowly while shaking with a lead rod for 10 minutes until the solution color changed to rosy black. Afterward, 3 ml of hydrogen peroxide ($H_2O_2$, 50%) was dropped slowly into the solution mixture until the color changed from rosy black to yellowish-orange. The precipitate was filtrated out, followed by cleaning four to six times with ethanol and deionized water by using Whatman filter paper (diameter 125 mm, thickness 200 µm, pore size 2.5 µm), and dried the filtrate in a vacuum oven at 70 ºC for 12 h. Figure 2.4a shows the transmission electron micrographs depicting the morphology of as-synthesized graphene oxide (GO).

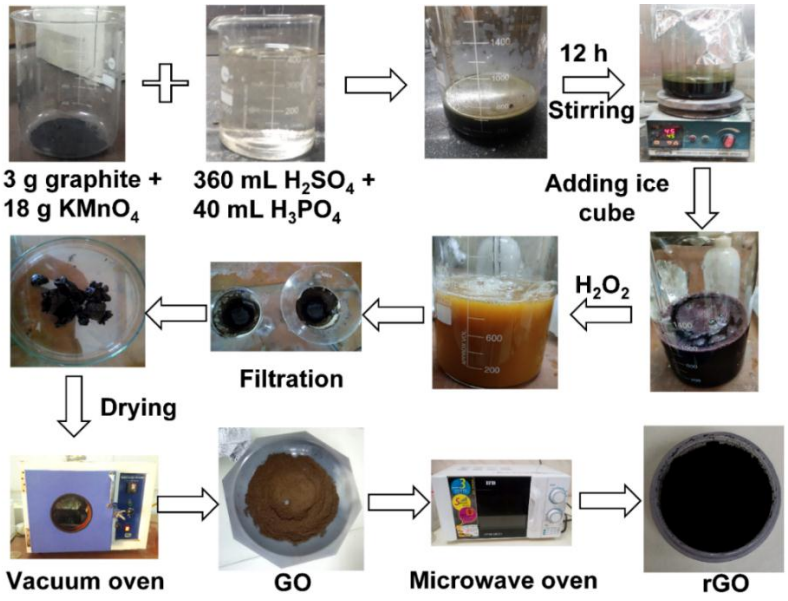


***Figure 2.3:*** *Step-by-step Synthesis of Graphene oxide (GO), and reduced graphene oxide (rGO) by using the modified Hummers' method.*

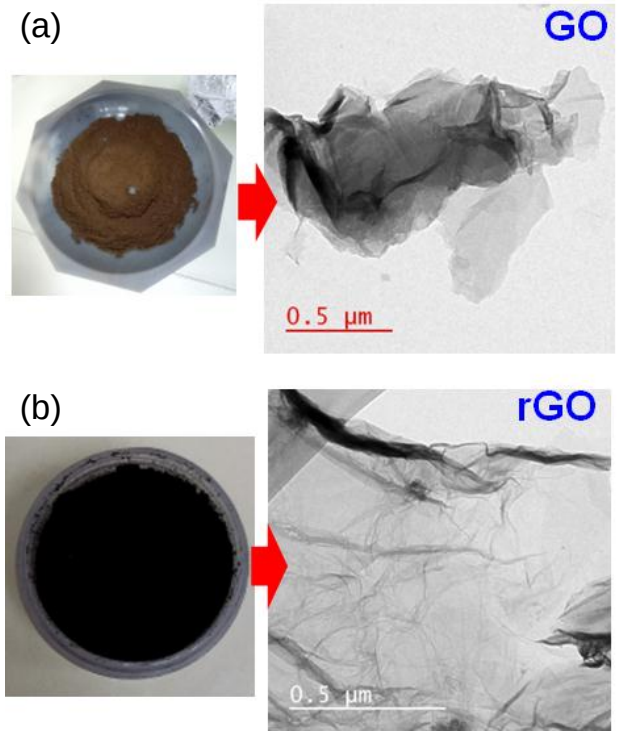


***Figure 2.4:*** *Shows the transmission electron micrographs of graphene oxide (GO), and reduced graphene oxide (rGO) by using the modified Hummers' method followed by microwave heat treatment.*

### 2.1.4 Synthesis of reduced graphene oxide (rGO)

The as-synthesized GO was taken in a glass crucible and heated in a microwave oven at 750 W for 30 min to produce reduced graphene oxide (rGO), as shown in Figure 2.3 [3]. Figure 2.4b shows the transmission electron micrographs depicting the morphology of as-synthesized reduced graphene oxide (rGO).

### 2.1.5 Synthesis of $MoNi_4/MoO_2$:rGO nanocomposite

The $MoNi_4/MoO_2$:rGO nanocomposite was synthesized by the one-pot hydrothermal process, as shown in Figure 2.5. In this typical process, 64 mg of as-synthesized rGO were mixed with 178 mg nickel (II) nitrate hexahydrate ($Ni(NO_3)_2.6H_2O$) and 187 mg ammonium molybdate tetrahydrate ($(NH_4)_6Mo_7O_{24}.4H_2O$) were dissolved in 30 ml of DI water and stirred for 20

min at 400 rpm for obtaining a clear solution. After that, 30 ml solution was transferred to 50 ml Teflon-lined autoclave and heated to 150 °C for six (6) h in an electric oven to complete the reaction. Afterward, the autoclave was allowed to cool down to room temperature (RT) naturally. Finally, the solution was cleaned with ethanol and DI water three times, followed by drying at 80 °C for 12 h in a vacuum oven. The as-synthesized powder sample was heat-treated in $H_2$:$N_2$ (5:95) gas environment at 500 °C for two (2) h to obtain rGO-supported $MoNi_4/MoO_2$ nanorods.

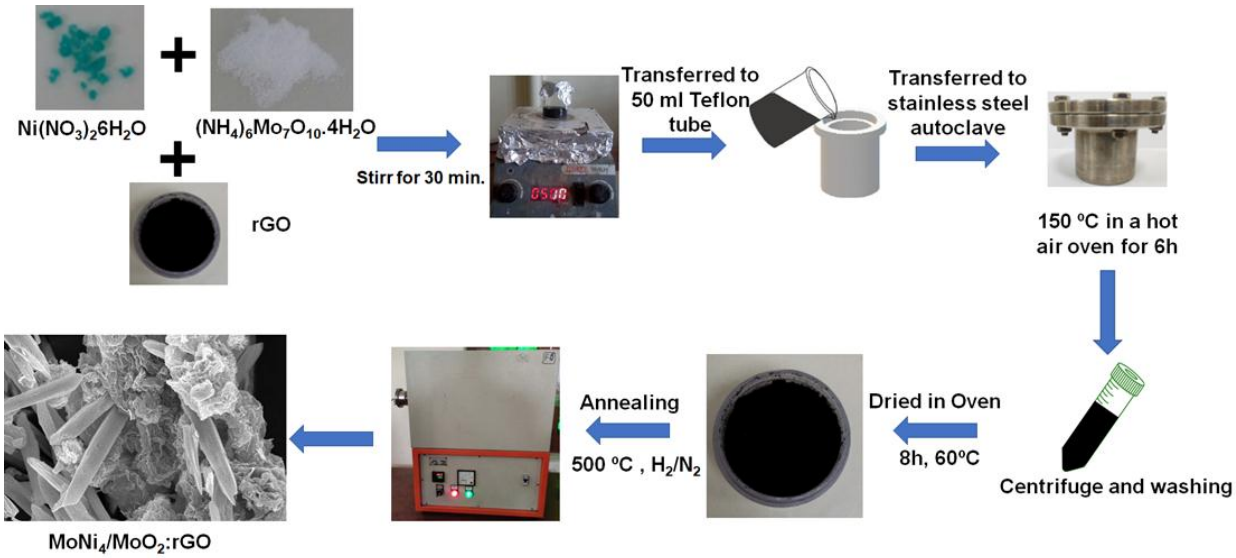


***Figure 2.5:*** *Schematic showing the step-by-step synthesis of $MoNi_4/MoO_2$:rGO nanocomposite.*

### 2.1.6 Synthesis of 2D-$MoS_2$ nanosheets via hydrothermal method

Two-dimensional (2D) $MoS_2$ nanosheets were synthesized using the hydrothermal method, where 3.8 g of thiourea ($CH_4N_2S$) and 2.067 g of ammonium molybdate tetrahydrate ($(NH_4)_6Mo_7O_{24}\cdot 4H_2O$) were dissolved in 60 mL of deionized water (DI water) which is shown in Figure 2.6. The as-prepared solution was stirred in a magnetic stirrer for 30 minutes to get a wholly dispersed solution, and then the reaction mixture was transferred to a 100 mL Teflon-lined autoclave and kept in a hot air oven at 180 °C for 24 hours. After 24 hours, the

autoclave was taken out and then naturally cooled down to room temperature. Then, the prepared solution was taken into a centrifuge tube and three to four times cleaned with a mixture of absolute ethanol and deionized water (DI water) at 7000-8000 rpm. The obtained product was dried in a vacuum oven at 80 °C to remove residual solvent for 12 hours.

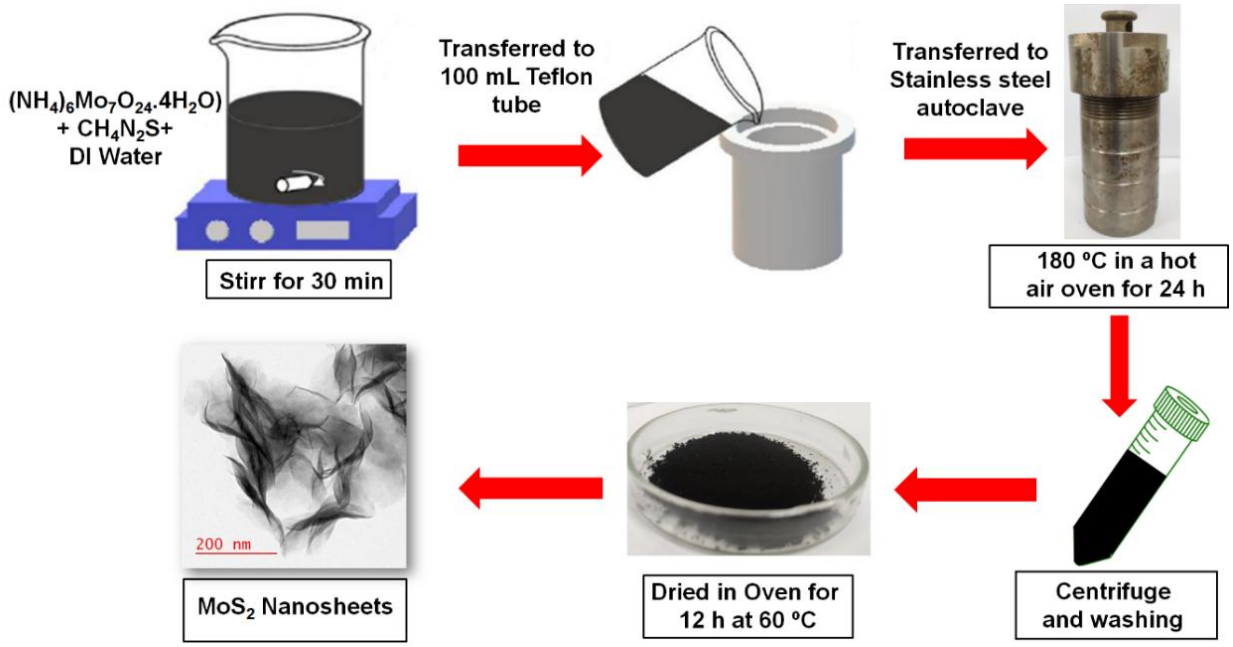


***Figure 2.6:*** *Schematic of the 2D-$MoS_2$ synthesized by a one-pot hydrothermal process.*

### 2.1.7 Synthesis of $MoS_2$:$MoNi_4/MoO_2$ nanohybrids

We used in-situ one-pot hydrothermal synthesis process for hybrid structure growth and 68 mg of ammonium molybdate tetrahydrate ($(NH_4)_6Mo_7O_{24}\cdot 4H_2O$), and 126 mg of thiourea ($CH_4N_2S$) were dissolved in 60 mL of DI water. After that, 50 mg of as-synthesized (as discussed in section 2.1.2) $MoNi_4/MoO_2$ powder was dispersed in the solution mixture, followed by stirring of the solution for 45 min at 500 rpm [1]. Next, the solution was moved to a 100 mL Teflon-lined autoclave and heated at 180 °C for 24 h in a hot-air oven. Once the reaction was completed, the Teflon-lined autoclave was allowed to naturally cool down to room temperature. Finally, the solution was washed with de-ionized water and dried at 80 °C for six (6) h inside of a vacuum oven to obtain $MoS_2$:$MoNi_4/MoO_2$ nanohybrid powder

(Figure 2.7). An identical synthesis process was followed to prepare pure 2D-$MoS_2$ powder via a hydrothermal method (Figure 2.6) without dispersing $MoNi_4/MoO_2$ powder in the solution.

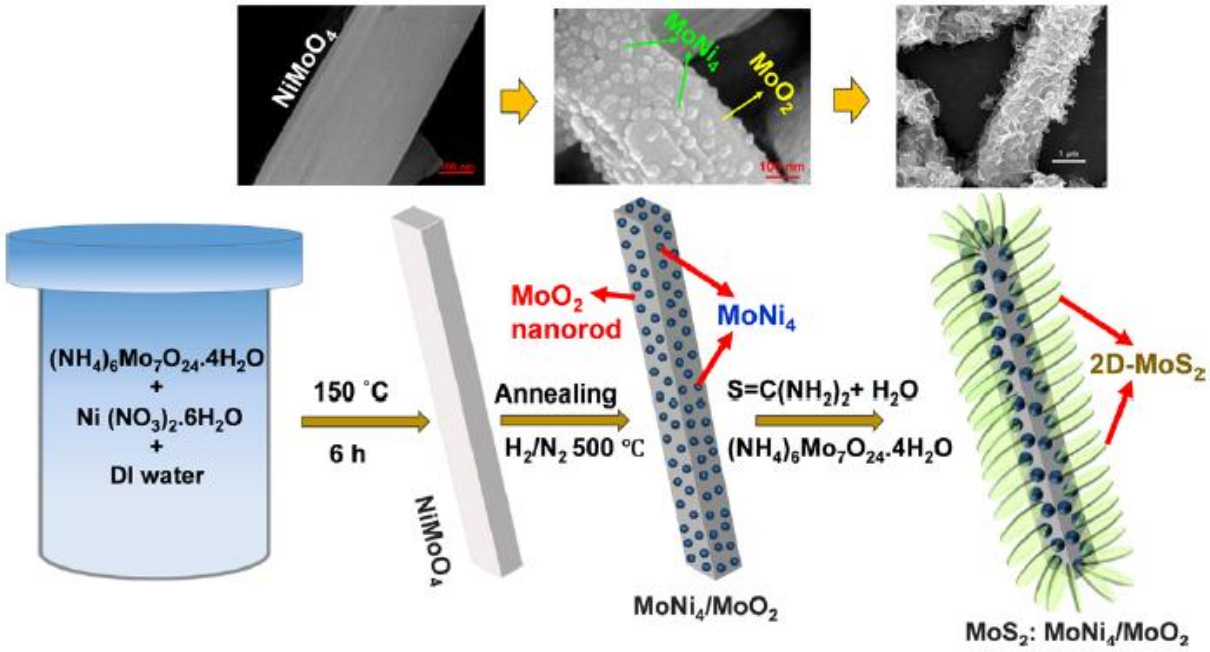


***Figure 2.7:*** *Schematic of the step-by-step Synthesis of $MoS_2$:$MoNi_4/MoO_2$.*

### 2.1.8 Synthesis of sulfonic acid ($SO_3H$) functionalized 2D-$MoS_2$ nanosheets

The $SO_3H$ functionalized $MoS_2$ nanosheets were synthesized by the one-pot hydrothermal method, as shown in Figure 2.8. In the typical process, about 2.067 g ammonium molybdate tetrahydrate $(NH_4)_6Mo_7O_{24}.4H_2O$ and the different precursor molar ratios of (2, 4, 6, 8, and 10) thiourea ($CH_4N_2S$) were first dissolved in 60 ml DI water. After that, the solution was stirred for 30 min at 250 rpm to get a transparent solution. Then, the solution was transferred to a 100 ml Teflon-lined stainless-steel autoclave tightly sealed and maintained at 180 ˚C for 24 h in a hot air oven. Once the reaction was over, the Teflon autoclave was naturally cooled down to room temperature. After cooling to room temperature naturally, the resulting black precipitate was separated by centrifugation at 7500-8500 rpm, followed by washing four

times with absolute ethanol and DI water, respectively, and dried at 80 ˚C for 12 h in a vacuum oven to obtain a powder.

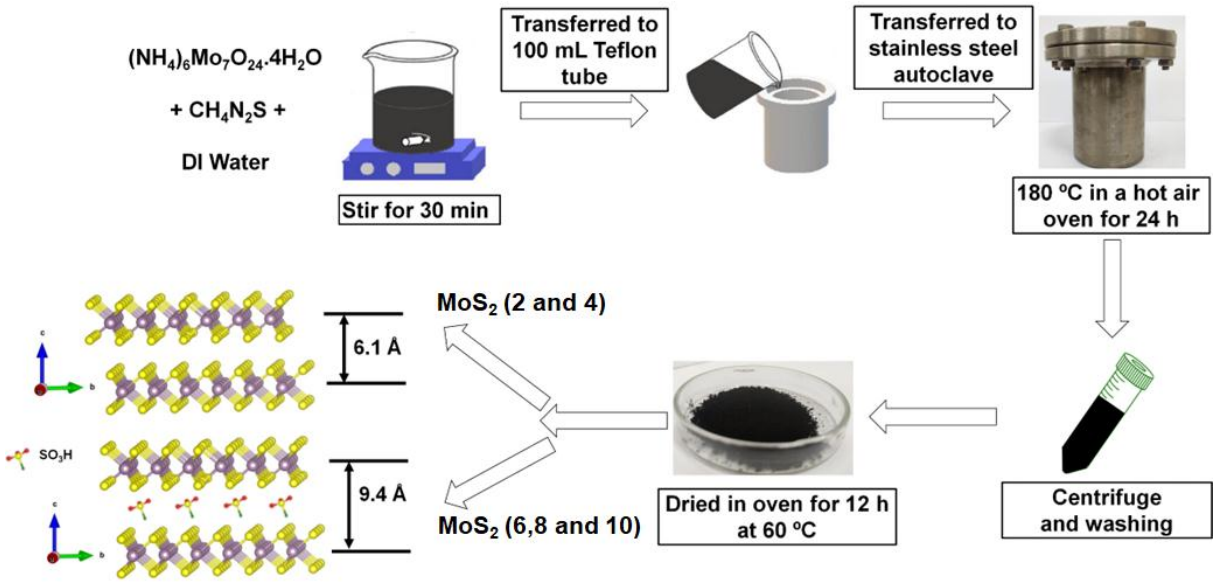


***Figure 2.8:*** *Schematic showing the step-by-step synthesis of $MoS_2$ and functionalized $MoS_2$ nanosheets.*

### 2.1.9 Sulfonic acid/ Sulfur trioxide ($SO_3H/SO_3$) functionalization in 2D-$MoS_2$ nanosheets

The $SO_3H/SO_3$ functionalized $MoS_2$ nanosheets were synthesized by a hydrothermal process (Figure 2.9). In the typical process, about 2.067 g ammonium molybdate tetrahydrate ($H_{24}Mo_7N_6O_{24}.4H_2O$) and 8.9 g thiourea ($CH_4N_2S$) were first dissolved in 60 ml DI water. After that, the solution was constantly stirred for 20 min at 400 rpm to get a transparent solution. Then the solution was transferred to a 100 ml Teflon-lined stainless-steel autoclave tightly sealed and maintained at 180 ˚C for 24 h in an electric oven. Afterward, the Teflon autoclave was cooled down naturally to room temperature (RT). After cooling, the resulting black solution was separated by centrifugation at 8000 rpm, followed by washing three times with ethanol and deionized water (DI) respectively, and dried at 80 ˚C for 12 h in a vacuum oven to obtain $SO_3H/SO_3$ functionalized MoS2 nanosheets.

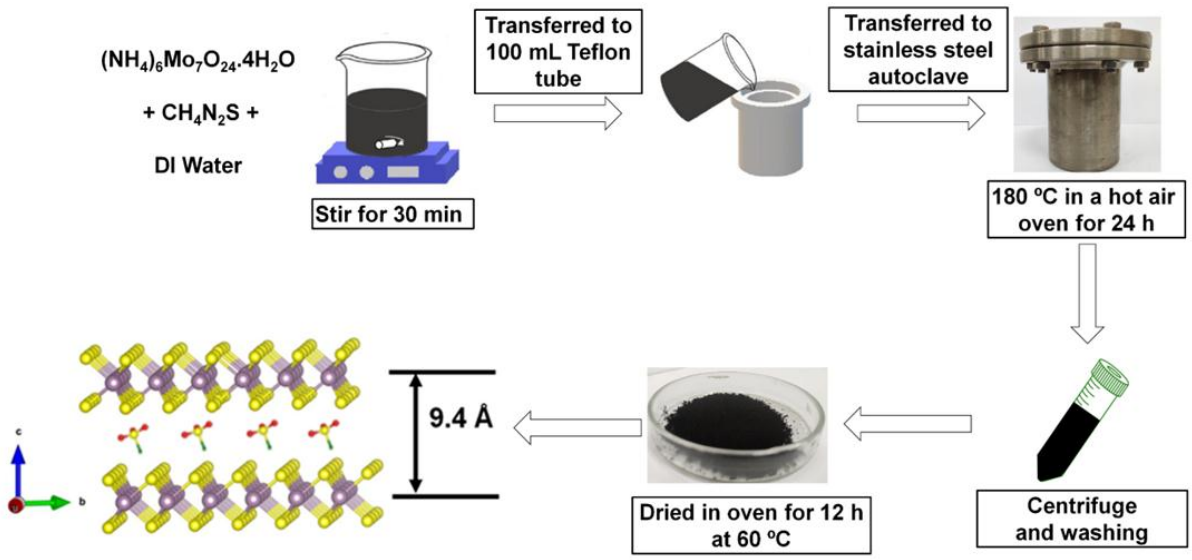


***Figure 2.9:*** *Schematic showing the step-by-step synthesis of $SO_3H/SO_3$ functionalized $MoS_2$ nanosheets.*

## 2.2 Techniques of materials characterizations

Different characterization techniques were used to characterize the as-synthesized nanostructured/functional nanostructured samples.

### 2.2.1 X-ray powder diffraction (XRD)

The structural and phase analysis of all as-synthesized powder samples was carried out in Rigaku Miniflex 600 powder x-ray diffractometer (RIGAKU Corporation, Japan) by using Cu-$K_\alpha$ radiation of wavelength 0.154 nm with the step size of 0.02º from 2θ = 5 to 80º and the generator functioned at 40 kV and 15 mA. All of the diffraction peaks were identified using the standard line profile in the JCPDS database. The interplanar d-spacing and particle size of the all as-synthesized powder sample were calculated by using Bragg's and Scherrer equation [4].

Bragg's equation $$n\lambda = 2dSin\theta \qquad (2.1)$$

Where λ is the wavelength of the X-ray beam (0.154 nm), d is the interplanar distance and θ is the diffraction angle and respectively.

Scherrer's equation $$t = \frac{k*\lambda}{B*COS\theta} \quad (2.2)$$

Where K is the constant (0.89), λ is the X-ray wavelength (0.154 nm), B is the full width at half maxima (FWHM) and θ is the diffraction angle, respectively.


***Figure 2.10:*** *Shows the pictographic image of Rigaku (miniflex 600) X-ray Diffractometer.*

### 2.2.2 Scanning electron microscopy (SEM)

The surface morphology of the gold-coated as-synthesized powders was investigated by using a scanning electron microscope (SEM) equipped with an energy-dispersive spectrometer (EDS) (Nova Nano SEM 450, FEI, Inc., USA) operating at a voltage of 15 kV.

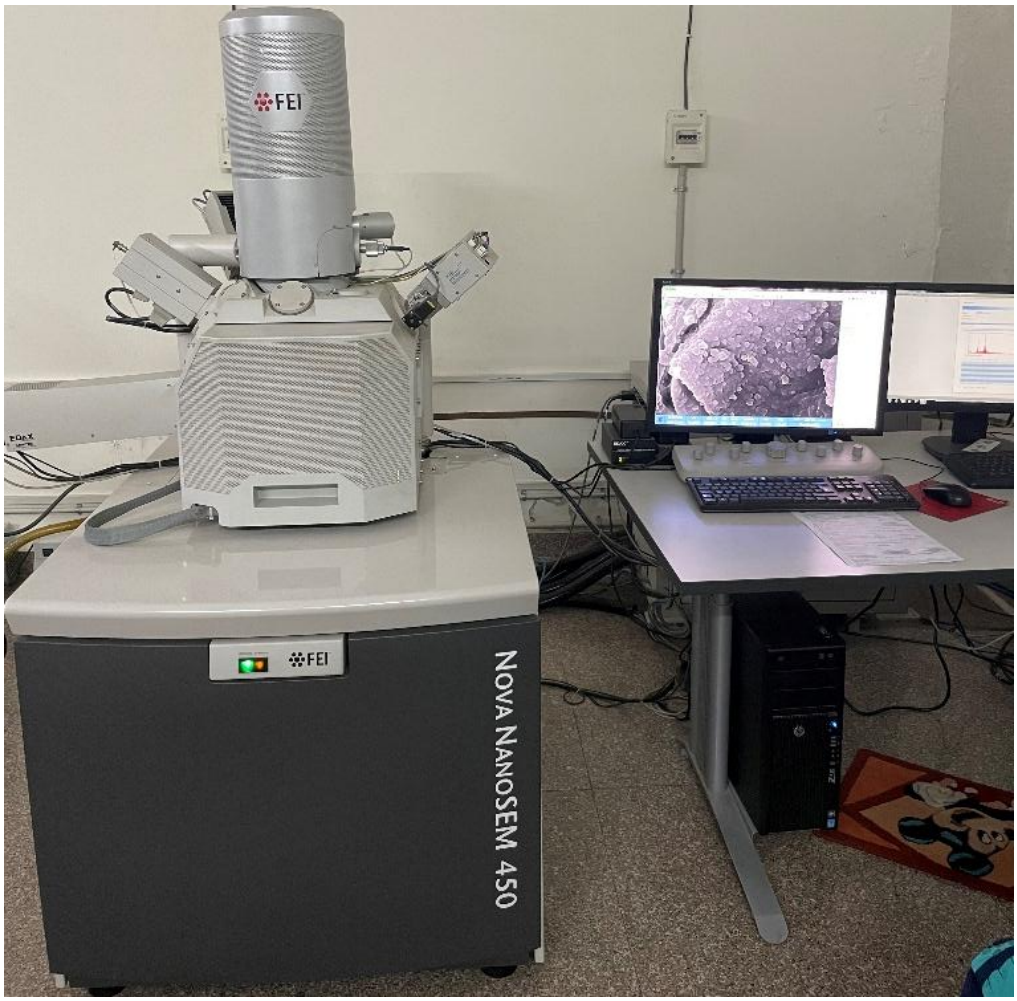


***Figure 2.11:*** *The field emission scanning electron microscope (Nova Nano SEM 450, FEI) equipped with the energy-dispersive spectrometer (EDS) mostly used for this research work.*

### 2.2.3 Transmission electron microscopy (TEM)

The morphology and phase of as-synthesized pristine and functionalized 2D nanostructure were investigated by using transmission electron microscopy (TEM) (TECNAI G2 20 TWIN, FEI-USA) equipped with the energy-dispersive X-ray spectroscopy (EDX) operating at a voltage of the 200 kV, where the as-synthesized powder sample was dispersed in ethanol and drop-cast on a carbon-coated 200-mesh TEM grid (SPi Supplies, USA). All TEM/HRTEM micrographs were analyzed by the Gatan software.

***Figure 2.12:*** *Shows a transmission electron microscope (TECNAI G2 20 TWIN, FEI-USA) equipped with the energy-dispersive X-ray spectroscopy (EDX) used for analyzing nanostructures for this research work.*

### 2.2.4. X-ray photoelectron spectroscopy (XPS)

X-ray photoelectron spectroscopy (XPS) is a surface sensitive spectroscopic technique that is used to provide information of the elemental composition, as well as the chemical and electronics state of as-synthesized samples near the surface of the material. In the XPS analysis, the sample is radiated with X-ray of fixed photon energy. Ionized photoelectrons will then be emitted from atomic and molecular orbitals of the target with a kinetic energy ($E_k$), which can be determined by the following equation [5].

$$E_b = \text{hv} - \varphi - E_k \qquad (2.3)$$

Where h is Planck's constant; $E_b$ is the binding energy of the ejected electron; υ is the frequency of the X-ray; $E_k$ is the kinetic energy of the ejected electron; φ is the work function of the spectrometer. The kinetic energies can be detected by the spectrometer. The characteristic $E_b$ can be used to identify the host element and thus the elemental composition of the surface can be qualitatively and quantitively studied. All as-synthesized functionalized 2D nanostructure chemical composition and oxidation state were investigated by using X-ray photoelectron spectroscopy (XPS) (K-alpha, XPS dispersive spectrometer, Thermo Scientific, USA) with an Al $K_\alpha$ monochromatic X-ray beam of energy 100-4000 eV and all of the measurements were carried out in the ultrahigh vacuum of ~$10^{-8}$ Torr pressure. All XPS data were analyzed by the CasaXPS software.

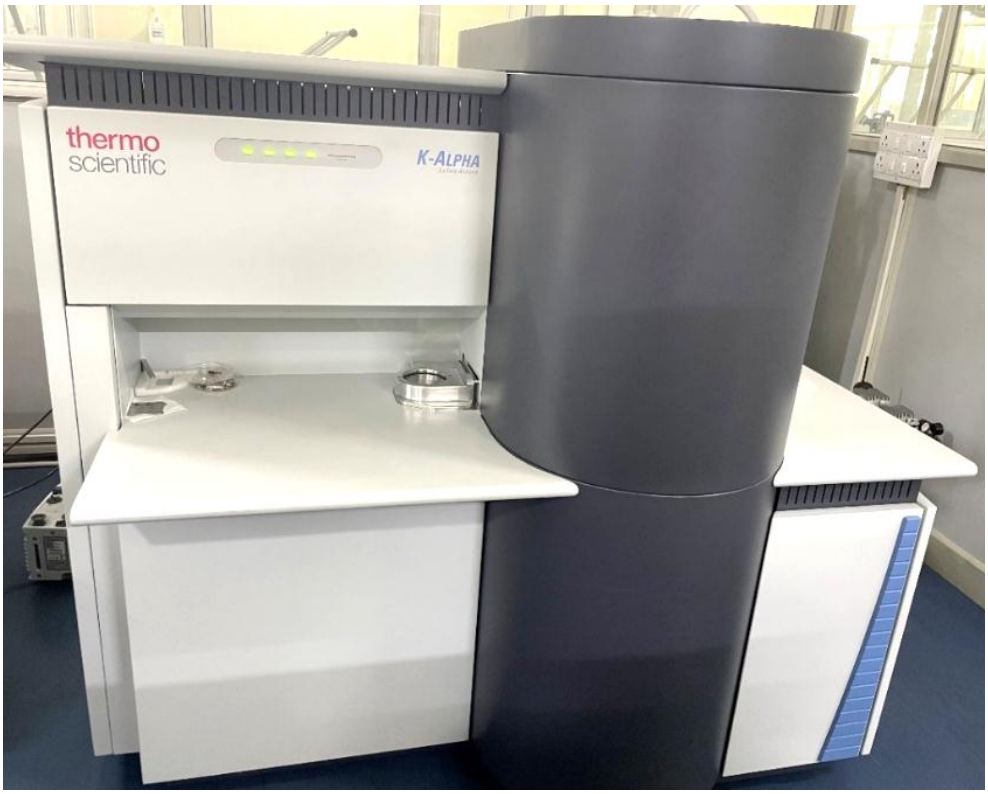


***Figure 2.13:*** *Shows the instrument for analysing X-ray photoelectron spectroscopy (XPS) (K-alpha, XPS dispersive spectrometer, Thermo Scientific).*

### 2.2.5 Raman spectroscopy

Raman spectroscopy is a technique used for fingerprinting and identifying the characteristic vibrational modes of 2D nanomaterials. The ratio of the different modes provides rich information on the texture of 2D nanomaterial layers. UHTS α-300 (WITec GmBH, Germany) confocal-Raman microscopy system with a 532 nm laser excitation at 1-2 mW power. Before measuring the sample, the Raman spectrometer was calibrated using a standard silicon chip (Si) to exclude any instrumental error. Spectra were typically taken with 50% filtered incident laser intensity from 200 to 2000 $cm^{-1}$ with a resolution of 1800 g/mm (1800 grooves per mm grating).

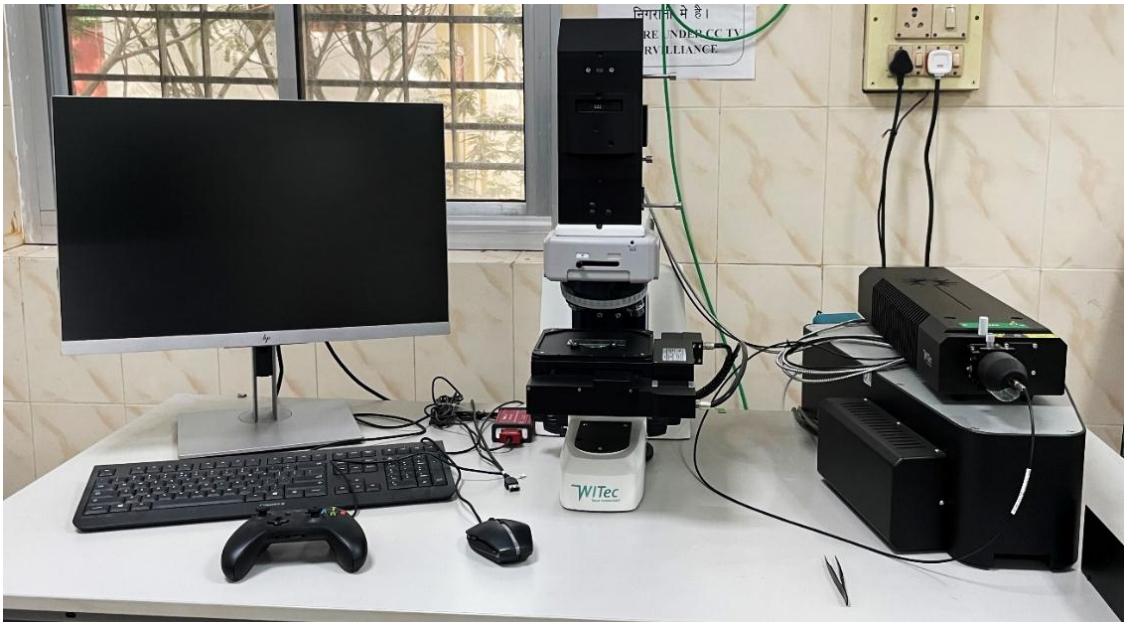


***Figure 2.14:*** *Confocal Raman microscopy system (UHTS α-300, WITec GmBH, Germany) in-built with a 532 nm laser source.*

### 2.2.6 Fourier transform infrared spectroscopy (FTIR)

The infrared spectrum of the samples was obtained by using an FTIR spectrometer (THERMO Electron Scientific, Instruments LLC, Model No: Nicolet iS5) from the ranges of 4000 to 400 $cm^{-1}$ with the resolution of ~ 4 $cm^{-1}$ were acquired.

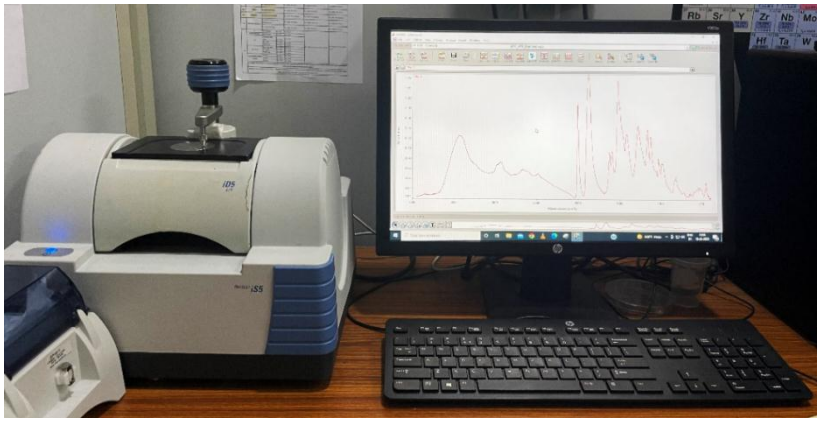

***Figure 2.15:*** *FTIR spectrophotometer (THERMO Electron Scientific, Instruments LLC, Model No: Nicolet iS5 instrument) used for all the FTIR measurements.*

### 2.2.7 Differential scanning calorimetry and thermogravimetric analysis

The thermal stability of as-synthesized powder samples was analyzed by the thermogravimetric analysis (TGA-50, M/s Shimadzu Pte Ltd.) technique from 30 ºC to 600 ºC in a Nitrogen gas was used to keep the environment inert, and scanned at the rate of 10 ºC/min. The different endothermic peaks of the as-synthesized powder sample were invested by using the differential scanning calorimetry (DSC-60 Plus, M/s Shimadzu Pte Ltd.) technique from 30 ºC to 550 ºC in a Nitrogen environment at the scan rate of 10 ºC/min.

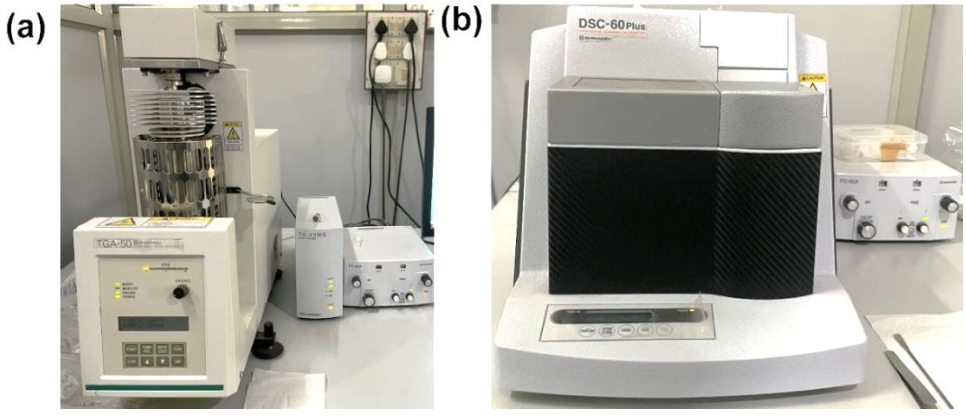


***Figure 2.16:*** *Shows pictographic images of (a) Thermogravimetric analysis (TGA-50, M/s Shimadzu Pte Ltd.) and (b) Differential scanning calorimetry (DSC-60 Plus, M/s Shimadzu Pte Ltd.) instrument.*

### 2.2.8 Ultraviolet-visible spectroscopy (UV-Vis)

Ultraviolet-visible spectroscopy **(**UV-Vis) spectroscopy is based on the absorption of light by a sample. UV-Visible spectrophotometer (Model No: V-770, JASCO, Japan) probes through the electromagnetic spectrum from ultraviolet through to the visible range (200-800 nm). Molecules often undergo electron transitions at these frequencies, since those molecules in question are semiconductors, which have energy levels corresponding to allowed electron states. The absorption spectra of the as-synthesized powder samples were further used to determine the bandgap of the semiconductor. The optical band gap of the as-synthesized powder sample was estimated by using the Tauc equation [6].

$$(\alpha h\nu) = B\ (h\nu - E_g)^n \qquad (2.4)$$

Where α is the absorption coefficient, ν is the photon frequency, B is a constant, h is the Planck's constant, $E_g$ is the bandgap and n can take the values that depend on the band gap type (1/2 and 2 for direct and indirect band gaps), respectively.

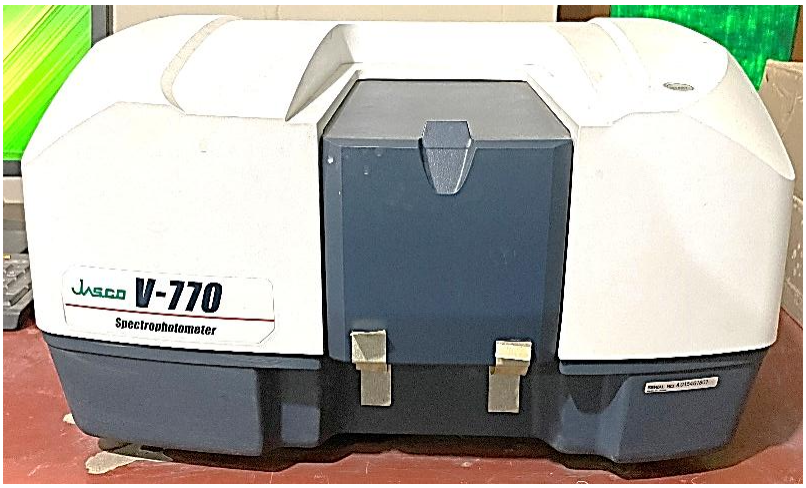


***Figure 2.17:*** *UV-Visible spectrophotometer (Model No: V-770, JASCO, Japan) used for all the UV-Vis measurements for this work.*

### 2.2.9 Brunauer-Emmett-Teller (BET)

The surface area of as-synthesized functionalized nanostructure was investigated by BET (Model- Autosorb IQ2, Quantachrome Instruments USA) (Brunauer, Emmett and Teller) measurement technique in liquid Nitrogen environment.

***Figure 2.18:*** *Autosorb IQ2 BET instrument for the surface area measurement.*

### 2.2.10 Contact angle measurement

The hydrophilicity and hydrophobicity of as-synthesised functionalized nanostructure were investigated by using optical tensiometer (Theto Lite, Biolin scientific). Eight (8) µl of water were drop cost on the surface of functionalized $MoS_2$ ($MoS_2$ palette) for the contact angle measurements.

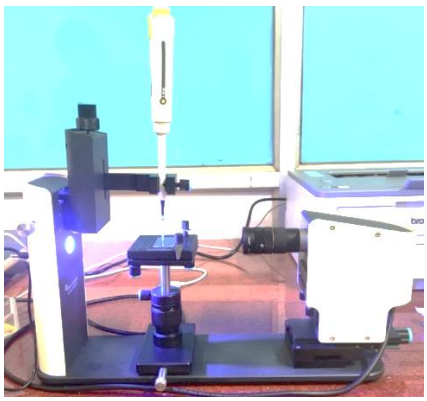

***Figure 2.19:*** *Optical tensiometer instrument for contact angle measurements.*

## 2.3 Electrochemical measurements

### 2.3.1 Electrode fabrication

All of the electrodes were fabricated by drop-casting the catalyst inks containing sample powders of as-developed functional nanostructures (Figure 2.20) [1]. The catalytic inks were prepared by adding 2.5 mg of the catalyst and 2.5 mg of Vulcan XC72 Carbon powder in 1060 µL of the solution, which was prepared by adding 60 µL of 5% Nafion, 500 µL of isopropanol, and 500 µL of DI water followed by sonication for 40 min to develop a homogeneous ink. The as-prepared inks were drop-cast on a graphite paper (GP) /Nickel foam within a constant effective area of 1 $cm^2$ followed by drying under ambient condition.

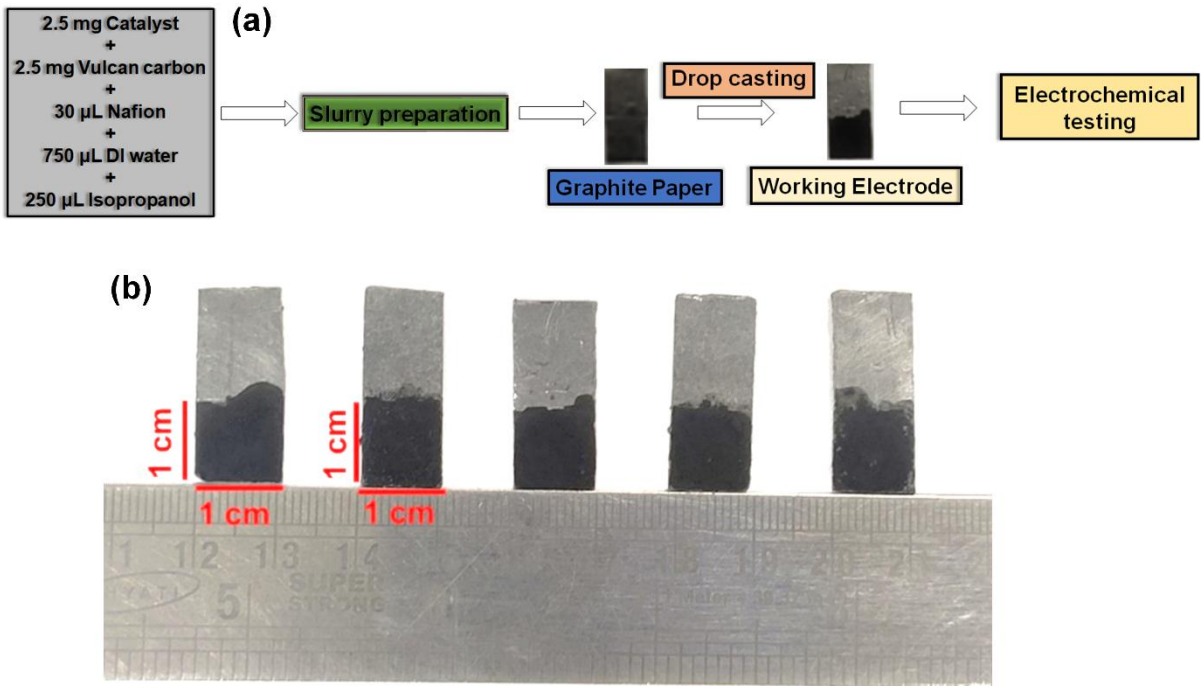


***Figure 2.20:*** *(a) Shows the step-by-step process for working electrode fabrication; (b) working electrode (WE) after the drop casting on 1 $cm^2$ graphite paper.*

### 2.3.2 Electrochemical characterizations

All the electrochemical measurements were performed with a modal AMETEK (Parstat 1000/2000A MC) dual-channel potentiostat/galvanostat inbuilt with impedance spectroscopy.

We also used another electrochemical workstation having potentiostat/galvanostat inbuilt with impedance spectroscopy from CorrTest (Model No CS350) in 1M KOH at room temperature. A three-electrode electrochemical cell configuration (Figure 2.21) was adopted for the measurement with saturated Ag/AgCl (std. 3M KCl) as a reference electrode (RE), a graphite rod was used as a counter electrode (CE), and the as-prepared catalysts-loaded graphite paper (as discussed in section 2.3.1) as working electrode (WE). For potentiodynamic polarisation, a 2 mV/s sweep rate was used. The potential was reported concerning RHE using the formula (Equation 2.5) [1, 7-9]:

$$E_{RHE} = E_{measured} + E_{Ag/AgCl} + 0.059\,pH \qquad (2.5)$$

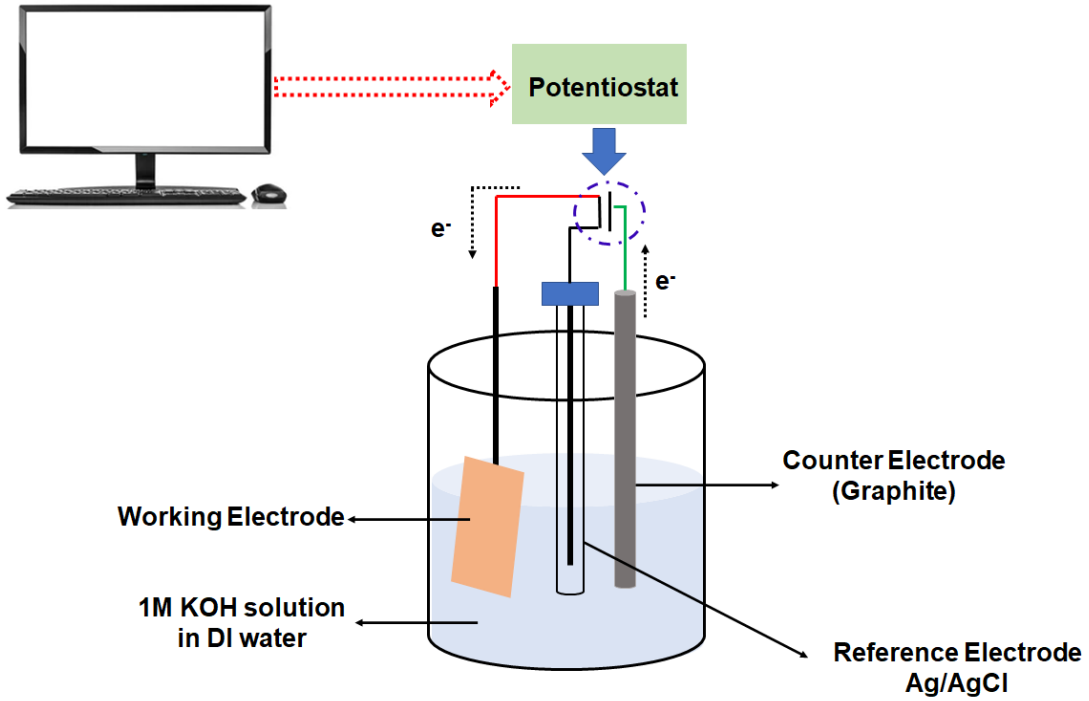


***Figure 2.21:*** *Schematic representation of a three-electrode system for electrochemical measurements. In this scheme, graphite and Ag/AgCl is used as a counter and reference electrode, respectively; and as-synthesized electrocatalytic electrodes on graphite paper/Ni foam were used as the working electrode for all the experiments.*

The electrochemical performance of water splitting with as-developed functional nanostructures was investigated by using four different types of measurements process: linear sweep voltammetry (LSV), electrochemical impedance spectra (EIS), cyclic voltammetry (CV), stability, and Mott-Schottky (M-S). All the electrochemical measurements were done as per the component shown in Figure 2.22.

### 2.3.2.1 Linear sweep voltammetry (LSV)

Linear sweep voltammetry (LSV) was carried out to identify the two important parameters (e.g., current density and overpotential) of hydrogen evolution reaction (HER) [7]. The LSV is a voltammetric measurement technique to analyzed the current density at a working electrode based on the overpotential. The polarization curves were obtained between the applied DC biases of ~ -0.2 V to-0.7 V vs. [Ag/AgCl] in 1 M KOH solution with a scan rate of ~ 2 mV/s, which were all corrected for the *i*R compensation.

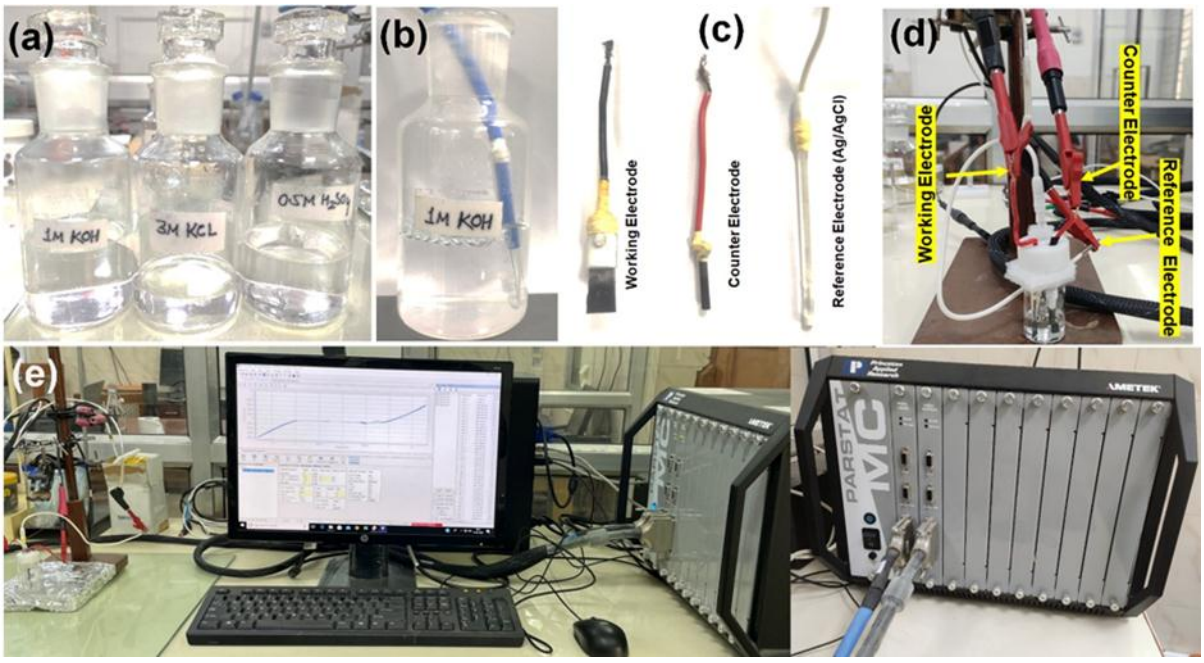


***Figure 2.22:*** *(a) Different electrolytes used during the electrochemical measurements; (b) Ar gas purging of any of the standard electrolyte solution before using it for electrochemical measurements; (c) represents the photographic images of different electrode (such as WE,*

*CE, RE) used for all these electrochemical measurements; (d) three-electrode arrangements for different electrochemical measurements; (e) AMETEK (PARSTAT, 1000/2000A MC) dual-channel electrochemical workstation, where all the electrochemical measurements were performed.*

**2.3.2.2 Electrochemical impedance spectroscopy (EIS)**

Electrochemical impedance spectroscopy (EIS) is an essential frequency-dependent technique often used to explore the interfacial behavior in electrochemical systems as a function of the alternating current (AC) (10 mV) with a variable frequency (1000 KHz to 0.1 Hz) at a constant potential -1.2 V (vs. RHE). The impedance of a system measured using this technique usually reveals the presence of two-time constants: high-frequency time constant and low-frequency time constant, which are often expressed graphically as Nyquist and Bode plots.[8] The EIS result offers the information regarding the interfacial reactions and electrode kinetics towards HER. In this work, the EIS was recorded with a frequency ranging from 1000 KHz to 0.01 Hz and perturbations were used for the measurements**.**

**2.3.2.3 Stability**

Stability is another important factor for evaluating the performance of the HER electrocatalysts for real-life use. Primarily, three techniques are there to test the HER stability, which include cyclic voltammetry (CV), chronoamperometry, and chronopotentiometry. Indeed, a slight change in the overpotential at the constant current density indicates better durability in acidic and alkaline medium. chronoamperometry/chronopotentiometry are the electrochemical characterizations, which measured the current density/potential over long-term HER operations as a function of time.

**2.3.2.4 Cyclic voltammetry (CV)**

Cyclic voltammetry (CV) was measured to calculate double-layer charging where, there is a linear correlation between double-layer charging and electrochemically active surface areas (ECSA). This means ECSA of the as-prepared electrodes could be estimated from the electrochemical double-layer capacitance ($C_{dl}$) of the catalytic surface. The ECSA of a catalyst sample was calculated from the double layer capacitance according to the Equation (2.6) [1].

$$C_{dl} = \frac{q}{v} \qquad (2.6)$$

Where $C_{dl}$ is the double-layered capacitance ($mF/cm^2$) of electro-active material, q is the charging current ($mA/cm^2$), and v is the scan rate (mV/s), respectively.[1]

$$ECSA = \frac{C_{dl}}{C_s} \qquad (2.7)$$

Where, $C_s$ is the specific capacitance of the sample or the capacitance of an atomically smooth planer surface of the material per unit area under the identical electrolyte conditions (0.04 $mF/cm^2$).

**2.3.2.5 Mott-Schottky (M-S)**

Mott–Schottky (M–S) was performed to understand the carrier density owing to the formation of a Schottky-junction barrier between the electrolytes and electrode. All the Mott-Schottky experiments were performed in 0.5M $Na_2SO_4$ (pH=7) electrolyte (i.e., neutral electrolyte) at frequency range 1000 Hz to 0.1 Hz from -1 to 1 V (vs. NHE) potential range. Theoretically, the slopes obtained from the Mott–Schottky data are used to evaluate the charge-carrier density of the electrode by using the following Equation (2.7) [9, 10].

$$N_d = (2/e\varepsilon\varepsilon_0)[d(1/C^2)/dE]^{-1} \qquad (2.7)$$

Where, $N_d$ is the carrier density, $\varepsilon$ represents the dielectric constant of the material, $e$ is the electronic charge unit ($1.602 \times 10^{-19}$ C), $\varepsilon_0$ denotes the permittivity of the vacuum ($\varepsilon_0$ = 8.85 with pH $\times 10^{-14}$ F $cm^{-1}$), and $E$ is the applied potential at the electrodes.

**References**


[1] V. K. Singh, U. Gupta, B. Mukherjee, S. Chattopadhyay, and S. Das, "$MoS_2$ Nanosheets on $MoNi_4/MoO_2$ Nanorods for Hydrogen Evolution," *ACS Applied Nano Materials,* vol. 4, no. 1, pp. 886-896, 2021, doi: 10.1021/acsanm.0c03296.

[2] D. C. Marcano *et al.*, "Improved Synthesis of Graphene Oxide," *ACS Nano,* vol. 4, no. 8, pp. 4806-4814, 2010, doi: 10.1021/nn1006368.

[3] R. Bhattacharyya, V. Kumar Singh, S. Bhattacharyya, P. Maiti, and S. Das, "Defect reconstructions in graphene for excellent broadband absorption properties with enhanced bandwidth," *Applied Surface Science,* vol. 537, p. 147840, 2021.

[4] "X-Ray Diffraction Methods," in *Materials Characterization*, 2013, pp. 47-82.

[5] "XPS Instrumentation," in *X- Ray Photoelectron Spectroscopy*, 2011, pp. 27-60.

[6] N. Saha *et al.*, "Highly active spherical amorphous $MoS_2$: facile synthesis and application in photocatalytic degradation of rose bengal dye and hydrogenation of nitroarenes," *RSC Advances,* vol. 5, no. 108, pp. 88848-88856, 2015.

[7] J. Zhu, L. Hu, P. Zhao, L. Y. S. Lee, and K.-Y. Wong, "Recent Advances in Electrocatalytic Hydrogen Evolution Using Nanoparticles," *Chemical Reviews,* vol. 120, no. 2, pp. 851-918, 2020.

[8] Z. Ge, B. Fu, J. Zhao, X. Li, B. Ma, and Y. Chen, "A review of the electrocatalysts on hydrogen evolution reaction with an emphasis on Fe, Co and Ni-based phosphides," *Journal of Materials Science,* vol. 55, no. 29, pp. 14081-14104, 2020.

[9] S. V. Singh, U. Gupta, B. Mukherjee, and B. N. Pal, "Role of electronically coupled in situ grown silver sulfides ($Ag_2S$) nanoparticles with $TiO_2$ for the efficient photoelectrochemical $H_2$ evolution," *International Journal of Hydrogen Energy*, vol. 45, no. 55, pp. 30153-30164, 2020.

[10] A. Ali *et al.*, "Ultrathin $MoS_2$ nanosheets for high-performance photoelectrochemical applications via plasmonic coupling with Au nanocrystals," *Nanoscale*, vol. 11, no. 16, pp. 7813-7824, 2019.